

Femtosecond laser fabrication of square pillars integrated Siberian-Cocklebur-like microstructures surface for anti-icing



Chengfang Ge^{a,b}, Gan Yuan^{a,b}, Chunlei Guo^c, Chi-Vinh Ngo^{a,*}, Wei Li^{a,b,*}

^a GPL, State Key Laboratory of Applied Optics, Changchun Institute of Optics, Fine Mechanics and Physics Chinese Academy of Sciences, Changchun 130033, China

^b University of Chinese Academy of Sciences, Beijing 100049, China

^c The Institute of Optics, University of Rochester, Rochester, NY 14627, USA

ARTICLE INFO

Article history:

Received 30 December 2020

Revised 1 March 2021

Accepted 28 March 2021

Available online 31 March 2021

Keywords:

Femtosecond laser ablation

Anti-icing

Siberian-Cocklebur-like microstructures

Polytetrafluoroethylene (PTFE)

ABSTRACT

In a low-temperature environment, water vapor in the ambient air is easy to condense and form frost on superhydrophobic surfaces, causing a reduction of their anti-icing performance. In this paper, a femtosecond laser was used to fabricate two new structures on polytetrafluoroethylene (PTFE) substrates to compare anti-icing properties with conventional structures. The two new structures are Siberian-Cocklebur-like microstructures and square pillars integrated Siberian-Cocklebur-like microstructures; whereas, the conventional structures include microgrooves with small step size, microgrooves with large step size, and square pillars. We illustrate the mechanism of forming the new structures in the interaction between the femtosecond laser and PTFE. The two new structures have greater water contact angles in a low-temperature environment than the conventional structures. We set up corresponding models for various microstructures contacted with water droplets and discuss hydrophobicity diversity. The two new structures on PTFE can effectively inhibit the vapor condensation in the microstructures and improve the hydrophobic performance and anti-icing property of PTFE surfaces in a low-temperature environment.

© 2021 The Author(s). Published by Elsevier Ltd. This is an open access article under the CC BY-NC-ND license (<http://creativecommons.org/licenses/by-nc-nd/4.0/>).

1. Introduction

Icing is a common phenomenon that causes much inconvenience to normal production and daily life. Several methods, such as chemicals treatment, mechanical vibration, electrothermal process, have been adopted for deicing [1]. However, those techniques come with environmental pollution, complex operation, and high energy consumption [2,3]. A new strategy that employs a superhydrophobic surface for anti-icing has attracted research's attention [4–6]. Water droplets can keep a good spherical shape on the lotus leaves' surface where it is easy to roll off, so it is not easy to be wetted by water droplets. Therefore, inspired by the effect of lotus leaves, superhydrophobic surfaces have been prepared [7–10]. A wax layer mainly governs the excellent hydrophobicity of lotus leaves with low surface energy and the papillary microstructures on the surface of lotus leaves [11]. The low surface energy and micro/nanostructured morphologies are the keys to produce artificial superhydrophobic surfaces. Generally, the superhydrophobic surfaces are defined with contact angles greater than 150° and

rolling angles less than 10° [12]. Superhydrophobicity can reduce the adhesion of the surface and make water droplets roll off easily before freezing and delay freezing time [13]. Ice adhesion strength with the superhydrophobic surfaces can be lowered as compared to smooth surfaces. Cao et al. demonstrated that superhydrophobic surfaces own the anti-icing ability, effectively preventing the ice accumulation on the surfaces [14]. It was observed that the anti-icing capability of superhydrophobic surfaces depends on the superhydrophobicity and the size of particles exposed on the surfaces. Ruan et al. prepared superhydrophobic anti-icing surfaces on the aluminum substrates by electrochemical anodic oxidation and chemical etching [15]. The superhydrophobic surfaces showed a lower freezing temperature (−6.1 °C) than those of the non-treated aluminum surfaces (−2.2 °C), which indicates the anti-icing property. Moreover, Guo et al. showed that the hierarchical micro/nanostructures could delay the freezing time and enhance the anti-icing performance of the surfaces compared to the single microstructures or the single nanostructures [16]. Surface chemical composition and morphologies play important roles in ice nucleation in a low-temperature environment. The small contact area between the water droplet and the surface reduces the heat transfer and the rate of heterogeneous nucleation at the interface so that superhydrophobic surfaces could delay the freezing time of the water droplet [17]. The research found that the freezing

* Corresponding authors at: GPL, State Key Laboratory of Applied Optics, Changchun Institute of Optics, Fine Mechanics and Physics Chinese Academy of Sciences, Changchun 130033, China.

E-mail addresses: chivinh@ciomp.ac.cn (C.-V. Ngo), weili1@ciomp.ac.cn (W. Li).

temperatures of small droplets (10 μL) reduce with the decrease of surface energy, while large droplets (300 μL) are independent in surface energy [18]. However, some studies have shown that the superhydrophobic surfaces do not always own the anti-icing capacity. For example, in a low-temperature and high-humidity environment, vapor in the air is easy to condense inside the microstructures of the superhydrophobic surfaces, which leads to the decrease of the hydrophobicity and the increase of the adhesion strength between the ice and the surface. As a result, the ice attached to the surface is more difficult to remove [19]. Another research showed that the delay of freezing time on a superhydrophobic surface is one order of magnitude higher than that of a superhydrophobic surface with nano roughness and high wettability [20]. Although the researches on anti-icing surfaces have been studied for several decades, the fabrication approach of environmentally friendly, low-cost, and excellent anti-icing performance surfaces still needs further studies [21].

Recently, femtosecond lasers have attracted extensive attention for their short pulse, high energy, and low thermal effect, which can be widely used to process micro/nanostructures on the surface of materials [22]. Among suitable polymers, PTFE can be chosen to become superhydrophobic by having micro/nanostructures on its intrinsically hydrophobic surface [23]. Moreover, it owns excellent properties such as high-temperature resistance, anti-acid, anti-alkali, and corrosion resistance [24]. It is still a great challenge to design and fabricate excellent anti-icing PTFE surfaces that could be widely used in industrial and daily lives in a low-temperature environment. At present, many typical line patterns and grid patterns with micro and nano hierarchical structures had been fabricated on the surface of PTFE by a femtosecond laser. However, the PTFE surfaces played a role as the mold surfaces [25,26]. Yin et al. fabricated multifunctional and robust near superamphiphobic polytetrafluoroethylene (PTFE) surface with hierarchical nano/microstructures by femtosecond laser, which exhibited anti-icing, anti-corrosion, and mechanical stability [27]. Chu et al. fabricated superamphiphobic surfaces with controllable adhesion by a femtosecond laser Bessel beam on PTFE, which showed anti-icing property [28]. However, the diversities of wettability and anti-icing properties between PTFE surfaces with different morphologies in a low-temperature environment have not been researched yet. Moreover, the hydrophobicity of structured PTFE surfaces will be decreased in the condensation and the formation of frost on the PTFE surfaces. Some even would lose superhydrophobicity which plays a significant role in anti-icing property in a low-temperature environment. Improving the anti-icing property of PTFE surfaces for practical applications in a low-temperature environment becomes an important issue.

In this paper, a femtosecond laser was employed to prepare superhydrophobic surfaces with different morphologies. By controlling laser energy, scanning speed, and scanning mode of laser, PTFE surfaces with various morphologies and dimensions have been successfully created. Herein, two excellent anti-icing property structures of PTFE surfaces inspired by Siberian cocklebur structures were created. They were Siberian-Cocklebur-like microstructures (SC), and square pillars integrated Siberian-Cocklebur-like microstructures (SP-SC). Moreover, several typical structures such as microgrooves with large step size (MLS), microgrooves with small step size (MSS), and square pillars (SP) were also created to have a comparison in properties with the two new structures. Hydrophobicity and anti-icing performances of these microstructural surfaces at low temperatures were then investigated and compared. The mechanism of forming new microstructures was explained based on the interaction between the femtosecond laser and PTFE. The wetting models of various structured surfaces in a low-temperature environment were set up. The theoretical calculation showed that SC and SP-SC surfaces

could reduce the contact area with water droplets, effectively delaying the freezing time. The relationship between contact angles and the freezing time of water droplets on different microstructural surfaces was compared. Furthermore, the influence of different micro morphologies on the anti-icing effect was investigated. Additionally, this study could propose a new direction for enhancing the anti-icing ability on surfaces by designing new morphologies and building corresponding wetting models for the wetting analysis in the low-temperature environment.

2. Experiment section

2.1. Preparation of different morphologies on PTFE

The femtosecond laser was directly used to write nano/microstructures on the PTFE surfaces, which simplified the preparation process of the superhydrophobic surfaces and improved the hydrophobicity of the PTFE surfaces. First, the PTFE plate was cut into small pieces with $15 \times 15 \times 1 \text{ mm}^3$. Second, the cut pieces were ultrasonically cleaned in an ethanol solution for 5 min and were then dried with nitrogen gas. A femtosecond laser (Spitfire Ace, Spectra Physics) was used in this research. The wavelength is 800 nm with a repetition rate of 1 kHz and a pulse width of 40 fs. The focal length of the focusing lens is 100 mm, and the aperture size is fixed at 7 mm. The radius of the focal spot produced by the Gaussian beam is roughly 9.463 μm . Last, the pieces were fixed on the 3D translation stage controlled by the software on the computer. After processing, the samples were ultrasonically cleaned in ethanol for 5 min. Fig. 1 describes a schematic of the femtosecond laser fabrication experimental setup, while Table 1 shows laser fabrication parameters for different structures in this research.

2.2. Characterization

The morphologies of PTFE surfaces were analyzed by a laser confocal microscope (Keyence, VK-X1000) and by a scanning electron microscope (Phenom, ProX800-07334). The wettability of samples was characterized by static contact angles and sliding angles, which were measured by a contact angle meter (POWER-EACH, JC2000D3). The volume of each water droplet was 6 μL .

Fig. 2 shows the schematic diagram of a self-built freezing time measurement device used to measure the freezing time of water droplets on PTFE surfaces with different morphologies. A cooling device was mainly used to cool the prepared samples with a thermoelectric cooler. An adjustable DC power supply mainly regulates the cooling power of the thermoelectric cooler. The temperature of the substrate was controlled by the output voltage of the power supply. The temperature of substrates was monitored in real-time through a thermocouple and temperature recorder contacted with a computer. The environment temperature and humidity were monitored by a temperature and humidity meter. The experiment was carried out under $23 \pm 2 \text{ }^\circ\text{C}$ temperature and $30 \pm 5\%$ humidity.

The prepared samples were placed on the surface of the substrate with thermal conductive silicone grease, covered with a glass culture dish. The temperature of the substrate was set at $-10 \text{ }^\circ\text{C}$. A deionized water droplet of 20 μL was placed on the sample surface. When the water droplet was placed on the surface of the sample, it was taken as the start time of the freezing process. When the water droplet was completely frozen and the top was pointed was taken as the end time of the freezing process. A camera was employed to record the whole operation process of this experiment. Five samples for each structured surface were fabricated. The presented data are average values.

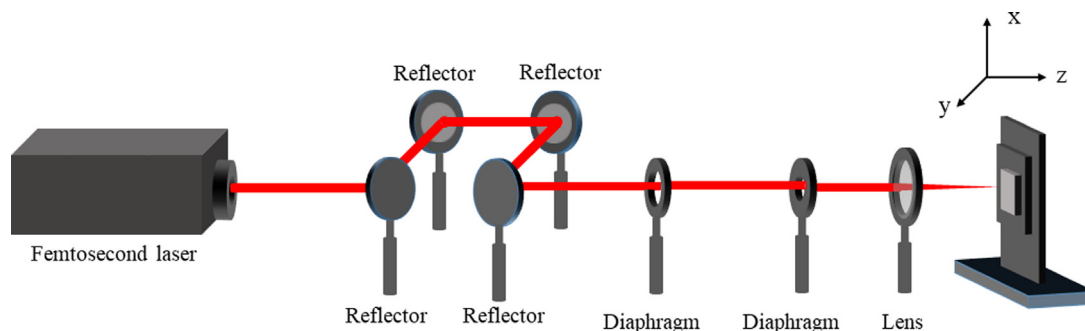


Fig. 1. Schematic experimental setup of femtosecond laser fabrication.

Table 1
Laser fabrication parameters of different structures on PTFE surfaces.

Structures	Laser power (mW)	Scanning interval (μm)	Scanning speed ($\text{mm}\cdot\text{s}^{-1}$)	Scanning mode
MLS	100	100	1	Transverse
MSS	25	25	2	Transverse
SP	100	100	1	Transverse and longitudinal
SC	25	25	2	Transverse and longitudinal
SP-SC	25 and 100	25 and 100	25 and 100	Transverse and longitudinal

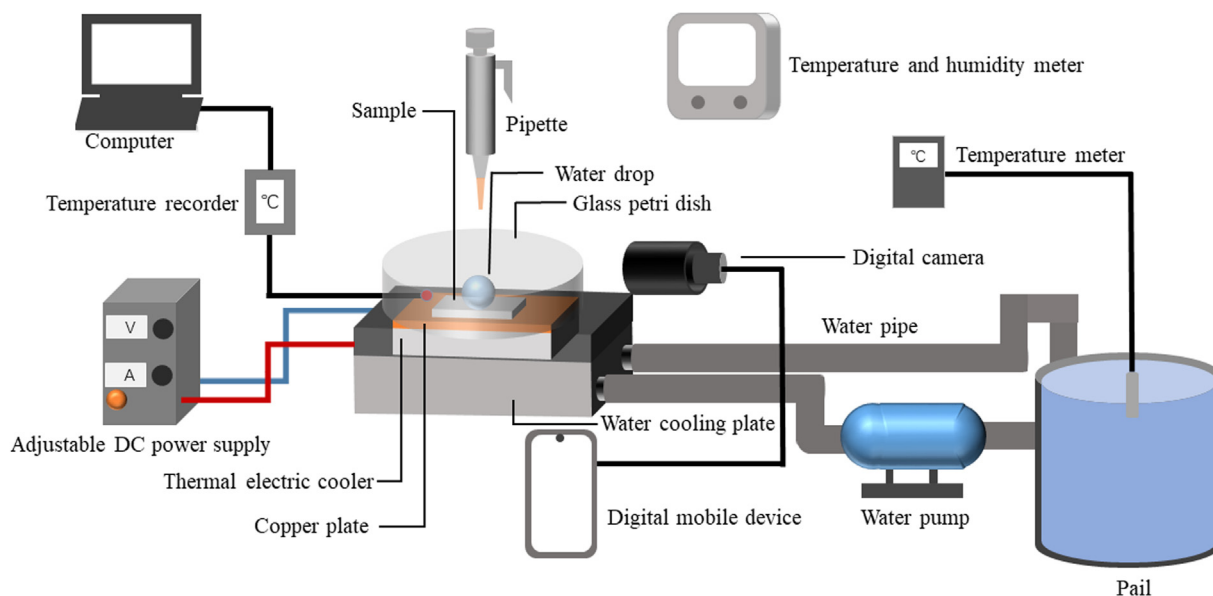


Fig. 2. Schematic of the system for testing freezing times.

3. Results and discussion

3.1. Morphologies of PTFE surface fabricated by femtosecond laser

Fig. 3 and Fig. 4 show the SEM images and confocal microscopy images of the PTFE surfaces with different morphologies, respectively. As we can see, the width of the groove increases with the increase of femtosecond laser power, which is due to the increase of average laser influence [25]. The depth of grooves increases with the decrease of the scanning speed of the femtosecond laser, which is due to the enhancement of the pulse accumulation effect [25,29]. The MLS and MSS micro-scale structures were fabricated by adjusting the interval of adjacent grooves, the laser power, and the scanning speed of the femtosecond laser. The size of microstructures could be fabricated by controlling scanning interval, laser power,

and scanning speed. For example, the width and the depth of the MLS microgrooves are about $45\ \mu\text{m}$ and $90\ \mu\text{m}$, respectively. However, the width and the depth of the MSS microstructures are roughly $20\ \mu\text{m}$ and $30\ \mu\text{m}$, respectively.

Additionally, SP and SC microstructures had been fabricated by transverse and longitudinal scanning. The width and the height of the SP microstructures are approximately $55\ \mu\text{m}$ and $90\ \mu\text{m}$, respectively. Interestingly, the small size SP microstructural surface was not fabricated but SC microstructural surface. The diameter of the bottom and the height of the SC microstructures are roughly $25\ \mu\text{m}$ and $16\ \mu\text{m}$, respectively. Fig. 5 shows the SEM images of SC and SP-SC microstructures at the magnification of 2000 times. It can be seen from the images that there are large amounts of burrs of several micrometers on the SC microstructures and the SP-SC microstructures.

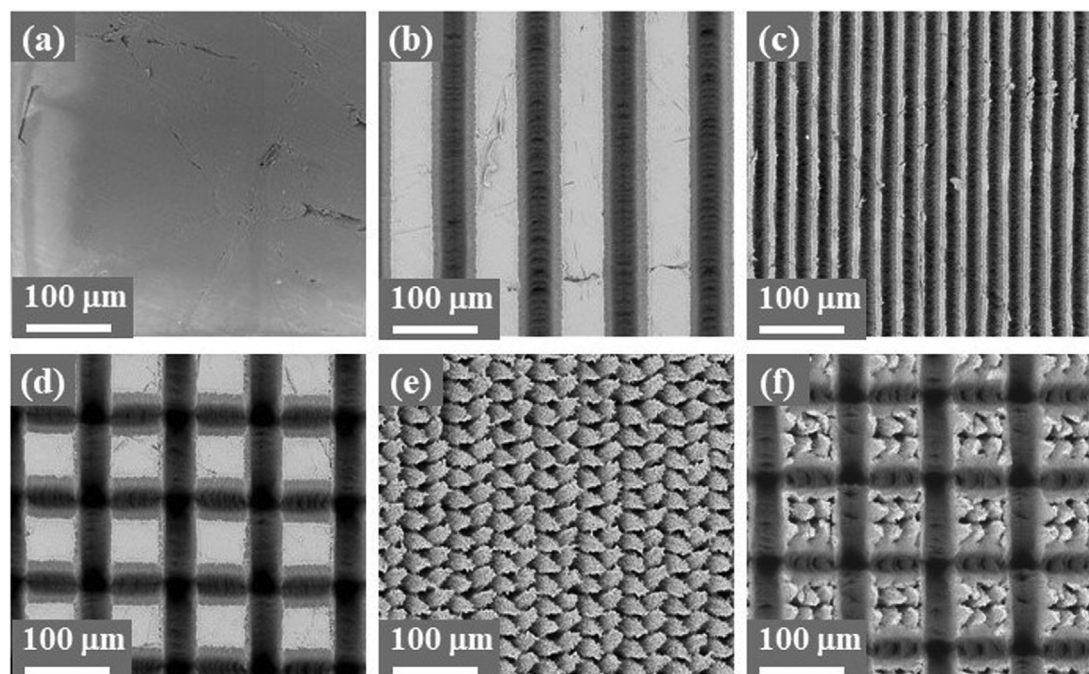


Fig. 3. SEM images of different PTFE surfaces: (a) Pristine, (b) MLS, (c) MSS, (d) SP, (e) SC, and (f) SP-SC.

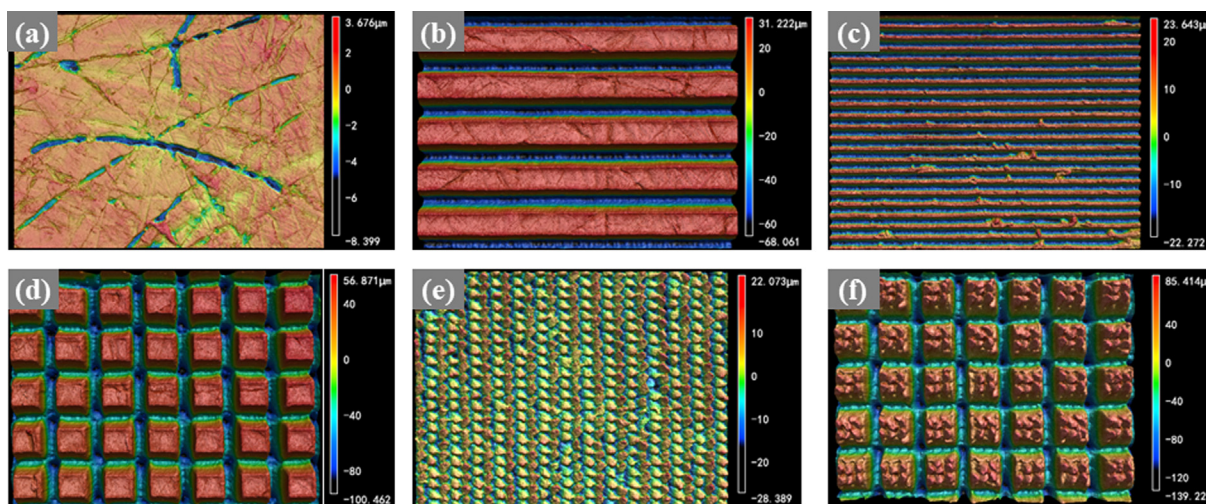


Fig. 4. Confocal microscopy images of different PTFE surfaces: (a) Pristine, (b) MLS, (c) MSS, (d) SP, (e) SC, and (f) SP-SC.

Moreover, the interaction between the femtosecond laser and the polymer surface is proposed. Since the laser pulses duration reaches the magnitude of the femtosecond, the femtosecond laser has high instantaneous peak power and owns the ability to ionize any material surface [30,31]. When the femtosecond laser interacts with the material surface, the focal volume will absorb the energy in the form of a nonlinear absorption mechanism, including multiphoton ionization and avalanche ionization [31]. Through ionization, free electrons absorb the energy of the laser and the kinetic energy of free electrons increases. High-temperature and high-pressure plasma come into being due to the transfer of energy from the electrons to the lattice. The ions of the melt phase begin to be vaporized, and then the plasma expands and rushes out of the focal volume because a large amount of kinetic energy is concentrated in the surface of material within the focal volume. The PTFE substrate begins to expand, melt and produce some gaseous products in the

process of femtosecond laser ablation [32,33]. The generated gas passes through the melting zone and spray from the body to the outer surface of the PTFE. As the laser irradiation spot moves forward, the molten polymer in the previous focal point volume instantly cools and solidifies, and the material near the laser focus can be removed and sputtered on the substrate. After that, the ablated area is covered with some particles when the ejected particles come back to the surface of the substrate and recrystallize [34].

Additionally, the energy distribution is high in the center and low in the edge for the Gaussian-profile of the femtosecond laser beam, so the fabricated grooves are more like a "V" shape [28,35]. When the femtosecond laser pulse irradiates PTFE, abundant fiber-like micro/nano hierarchical structures are formed on the ablated area of PTFE [25]. Through shortening scanning intervals between adjacent ablated track, the rate of the ablated area

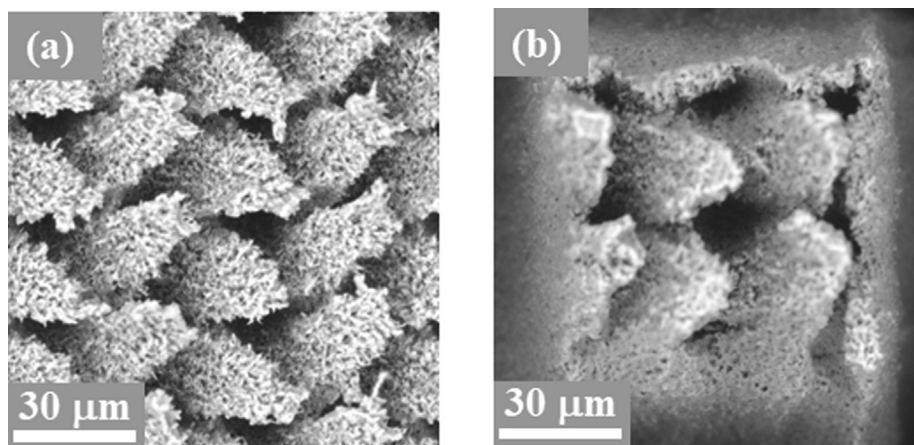


Fig. 5. SEM images of SC and SP-SC structures: (a) SC, and (b) SP-SC.

was increased. Besides, cross scanning of transverse and longitudinal cross scanning increases the ablated area further. Since laser fabrication scanning between two ablated routes is opposite, the directions between two adjacent trains of fabricated SC microstructures were also the opposite. As for SP-SC structures, it was fabricated by firstly fabricating SC structures and following with fabricating SP structures.

3.2. Effect of structure shapes to surface wettability at a room temperature

Fig. 6 shows the images of contact angles on the different morphologies of PTFE with 6 μL deionized water droplets. Fig. 7 shows the contact angles and sliding angles of different morphologies of PTFE. The error bars indicate the maximum and the minimum values of the measured data. The static contact angles of untreated (pristine) PTFE is 122°, presenting a hydrophobic property. During the measurement of rolling angles, some water droplets could not roll out of the surface due to the high adhesion force, so the rolling angle results are marked as 90° for better comparison to the samples with small sliding angles. The untreated (pristine) PTFE shows good hydrophobicity due to intrinsically low surface energy. The average values of the contact angles of MLS, MSS, SP, SC, SP-SC structures are 157°, 158°, 160°, 160°, and 158°, respectively. The average values of the sliding angles of MLS, MSS, SP, SC, SP-SC

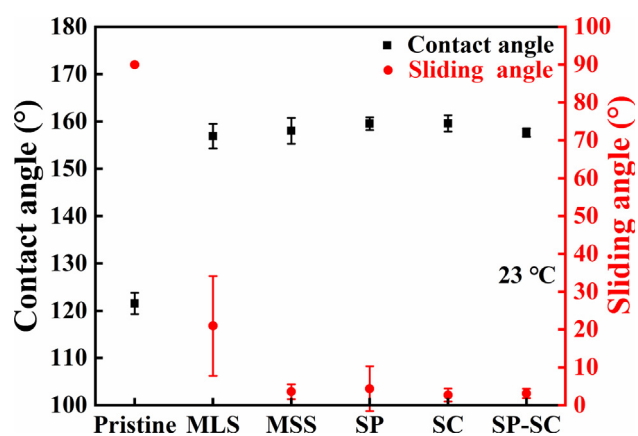


Fig. 7. Static contact angles and sliding angles of different PTFE structures at 23 °C.

structured surfaces are 21°, 4°, 4°, 3°, and 3°, respectively. As we can see, the static contact angles of structured PTFE surfaces processed by the femtosecond laser are more than 150°. Additionally, while the sliding angles of the MSS, SP, SC, SP-SC structured surfaces are less than 5°, the sliding angles of MLS structured surfaces are more than 10°. The results indicate that the hydrophobicity can be significantly improved by fabricating micromorphology on

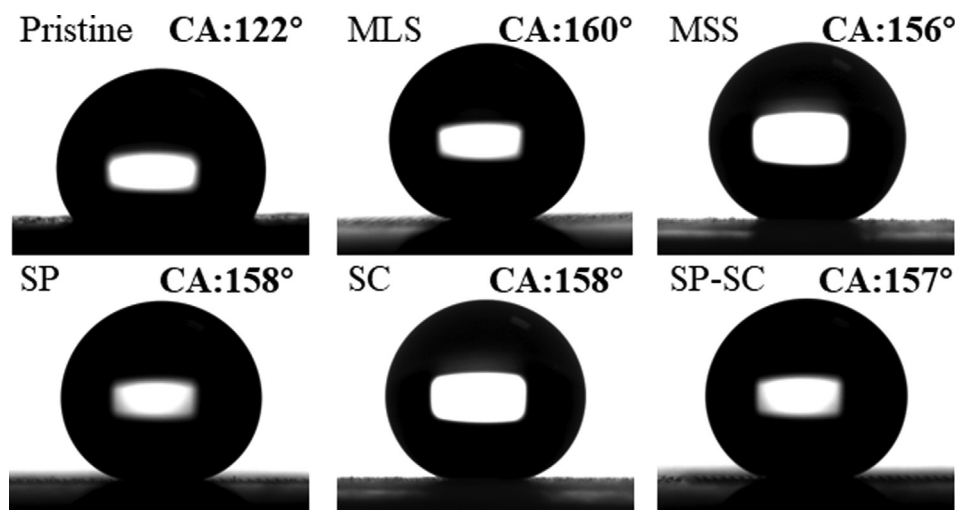


Fig. 6. Images of contact angles of PTFE with different structures at 23 °C.

intrinsic hydrophobic surfaces. Due to the low sliding angles and large contact angles between the water droplets and the structured surfaces, the wetting state of water droplets on these surfaces should be Cassie Baxter state, where the air gaps between the water droplets and the structured surfaces exist. A large amount of air is stored inside the microstructures of the PTFE surfaces indicates that there is a discontinuous three-phase contact surface among water droplets, the air inside microstructures, and the PTFE surfaces. This wetting state can significantly reduce the adhesion force of the surfaces, which makes it difficult for water droplets to adhere to the surface. Compared with other microstructural surfaces, the adhesion force between water droplets and the MLS surface increased slightly. This case is mainly due to large-scale microstructures; water droplets partly penetrate MLS grooves, and the contact state turns to a transition state [36].

According to the Cassie and Baxter equation, the contact angle can be described below.

$$\cos \theta_c = f_s \cos \theta_s + f_v \cos \theta_v \quad (1)$$

Where θ_c is the actual contact angle between the liquid and the surface, f_s is the percentage of the actual contact area between the liquid and the solid surface, f_v is the percentage of the actual contact area between the liquid and the air in the microstructures, θ_s is the intrinsic contact angle of the solid surface, θ_v is the contact angle of the air interface $f_s + f_v = 1$ and $\theta_v = 180^\circ$ then:

$$\cos \theta_c = f_s (\cos \theta_s + 1) - 1 \quad (2)$$

According to static contact angles measured and the Cassie and Baxter equation, we get the f_s through theoretical calculation. From the results given in the Table 2, f_s values of different morphologies show little difference at room temperature, which means the actual contact area between water droplets and PTFE surfaces is almost the same between these different morphologies. The hydrophobicity of the surface was mainly governed by the surface energy and morphology of the material [36]. Owing to low surface energy, the morphologies of the PTFE surface do not significantly impact hydrophobicity to a certain degree in a room temperature environment.

Moreover, anticorrosive property and mechanical stability of the SC and SP-SC structures were investigated to check the feasibility of working in harsh environments, as shown in Fig. S1 and Fig. S2. The results showed that SC and SP-SC structures could work in acids or bases environments with acceptable mechanical stability.

3.3. Effect of structure shapes to surface wettability at a low temperature

Fig. 8 shows the images of contact angles on the different morphologies of PTFE with 6 μL deionized water droplets at the surface temperature of -10°C . Fig. 9 shows the average contact angles and sliding angles on the different morphologies of PTFE with water droplets at the surface temperature of -10°C . The error bars indicate the maximum and the minimum values of the measured data. As we can see, the average value of static contact angles of untreated (pristine) PTFE is 102° , and the average value of sliding angles of untreated (pristine) PTFE is 90° . The average values of contact angles of MLS, MSS, SP, SC, SP-SC are 129° , 133° , 134° ,

148° , 150° respectively, at -10°C . The average values of sliding angles of MLS, MSS, SP, SC, SP-SC are 90° , 84° , 72° , 21° , 14° respectively, at -10°C . The hydrophobicity of different morphologies of PTFE at this low temperature decreased comparing to the hydrophobicity at room temperature. It is worth noting that the hydrophobicity of untreated (pristine), MLS, MSS, and SP decreased much while the hydrophobicity of SC and SP-SC decreased little, which indicates that SC and SP-SC can maintain good hydrophobicity at low temperatures.

According to the Cassie and Baxter equation (3), we define the contact angles of untreated (pristine) PTFE at low temperatures as the intrinsic contact angles, f_s values of different morphologies of PTFE at low are shown in Table 2. The f_s values of SC and SP-SC microstructures are lower than others, which indicates the contact areas between water droplets and the SC, SP-SC surfaces were reduced further compared to other structured surfaces in the low-temperature environment. Since the temperature of PTFE surfaces is below the freezing point, the supersaturation conditions are achieved. The condensation and frost nucleation can form in the post tops, sidewalls, and valleys without any aspatial preference indiscriminately on structured surfaces [37]. As shown in Fig. 10, condensation and frost nucleation on substrates means new surfaces are created on PTFE surfaces. The untreated (pristine) PTFE surface owns excellent hydrophobicity due to low surface energy in a room-temperature environment. However, the hydrophobicity of untreated (pristine) PTFE surface decreased due to the condensation and frost exposed on the surface at low temperature. This phenomenon happens as same as in the other microstructural surfaces. The hydrophobicity of all surfaces had been reduced, so the contact angles of all surfaces decreased, and the sliding angles increased. However, the surface of SC microstructures has abundant small-scale microstructures exposed on the surface, which can reduce the amount of frost on the tips of the microstructures and contact the water droplets. The surface of SC microstructures remains superhydrophobicity at -10°C . The SP-SC microstructures are the combination of SP microstructures and SC microstructures, which can reduce the contact area with water droplets much more than single SP and SC microstructural surfaces, so the hydrophobicity of the surfaces at -10°C has increased further. As a result, the f_s values of both SC microstructures and SP-SC microstructures are much lower than those of other microstructural surfaces.

Additionally, the smaller contact area and the air gap inside the microstructural surfaces reduce the heat transfer rate between the droplet and the surface, delaying the water droplet freezing at low temperatures. Besides, low surface energy and small contact area make the water droplets easy to roll down under external force action before freezing, so the sliding angles of water droplets are reduced, which can avoid the accumulation of ice in the low-temperature environment.

3.4. Anti-icing property

A camera records the freezing time taken for droplets to be frozen on the surface at -10°C . The freezing progress of water droplets on the PTFE surfaces with different morphologies is shown in Fig. 11. In the beginning, the water droplet on the surface is

Table 2

The percentage of the actual contact area between the liquid and the solid surface.

Temperature	The percentage of the actual contact area (f_s)				
	MLS	MSS	SP	SC	SP-SC
23 $^\circ\text{C}$	0.169	0.155	0.128	0.128	0.155
-10°C	0.468	0.401	0.385	0.192	0.169

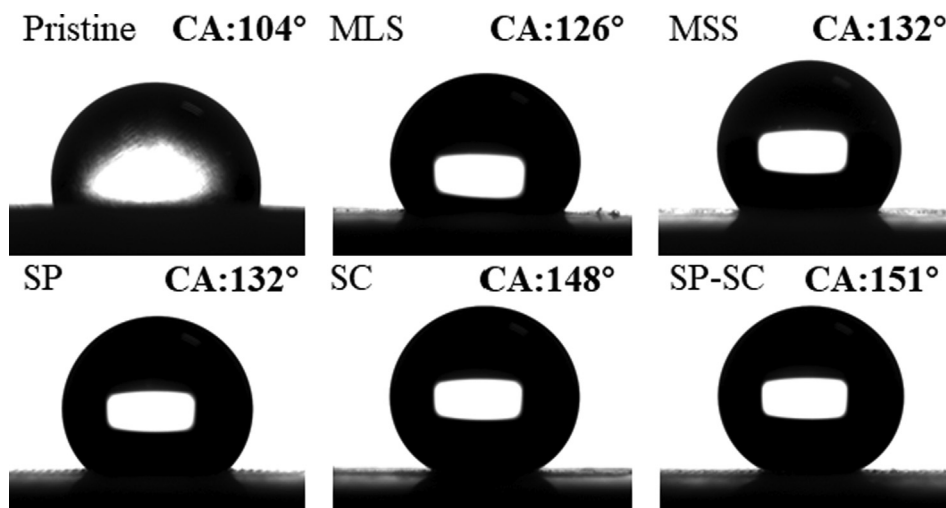


Fig. 8. Images of contact angles of PTFE with different structures at $-10\text{ }^{\circ}\text{C}$.

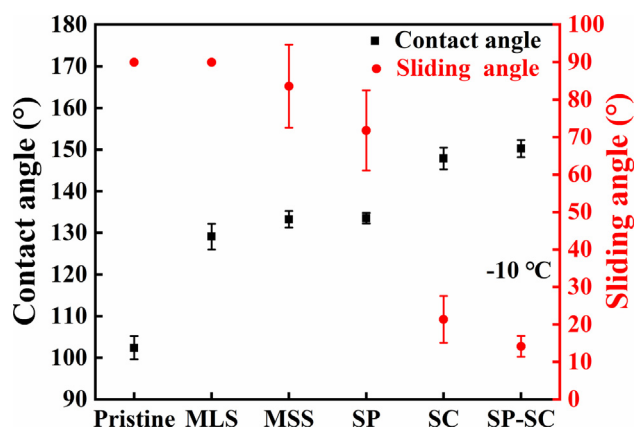


Fig. 9. Static contact angles and sliding angles of different PTFE structures at $-10\text{ }^{\circ}\text{C}$.

transparent. During the cooling progress, an ice shell forms at the surface of the droplet while the inter of the ice shell is still liquid [38,39]. After that, an ice-water interface forms and rises in the inter of the ice shell until the whole water droplet is frozen. When a cone with a small bulge appeared on the top of the droplet, the freezing progress ends.

The freezing time of the PTFE surface with different morphologies at low temperatures is shown in Fig. 12. The error bars indicate the maximum and the minimum values of the measured data. The freezing time of untreated (pristine) is 173 s. The freezing times of MLS, MSS, SP, SC, SP-SC are 271 s, 285 s, 297 s, 312 s, and 334 s, respectively. As we can see, superhydrophobic surfaces can delay the freezing time of water droplets at low temperatures. The freezing times of different morphologies are distinct. SC and SP-SC's freezing times are longer than other microstructural surfaces, which means SC and SP-SC microstructures own better anti-icing properties. The longer freezing time can provide more time for removing water droplets under external force and reduce the accumulation of a large quantity of ice on the surfaces. It is worth not-

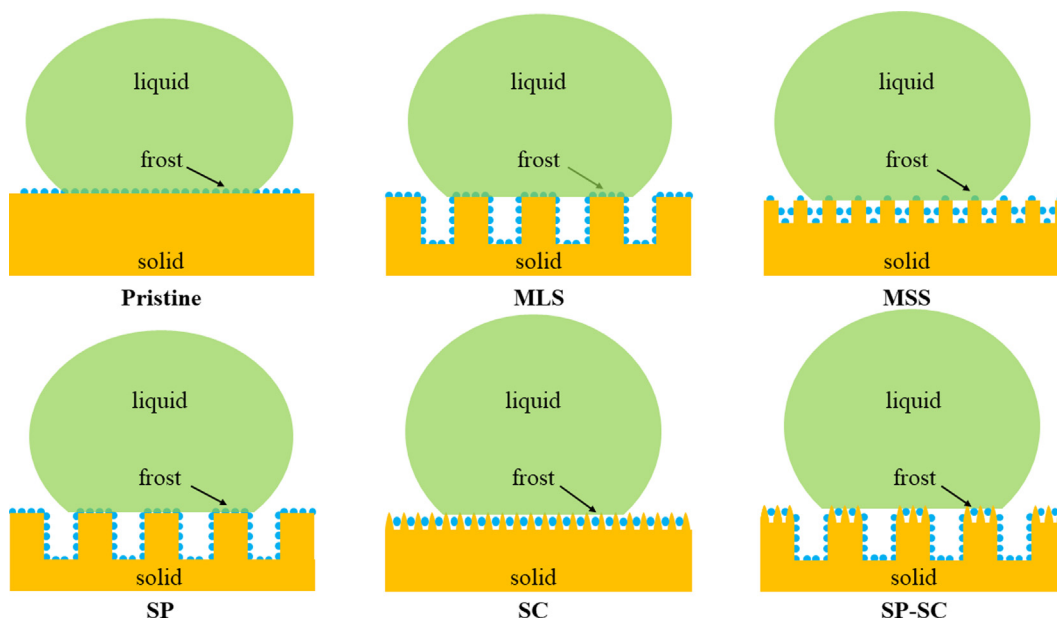


Fig. 10. Schematic of the liquid droplet in contact with the different PTFE surfaces.

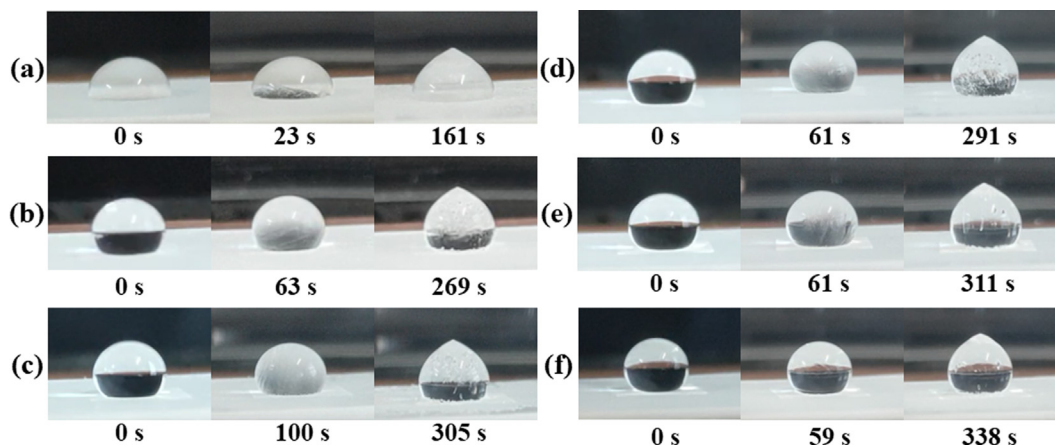


Fig. 11. The ice formation process of water droplets on different PTFE structures under $-10\text{ }^{\circ}\text{C}$ of temperature: (a) Pristine, (b) MLS, (c) MSS, (d) SP, (e) SC, and (f) SP-SC.

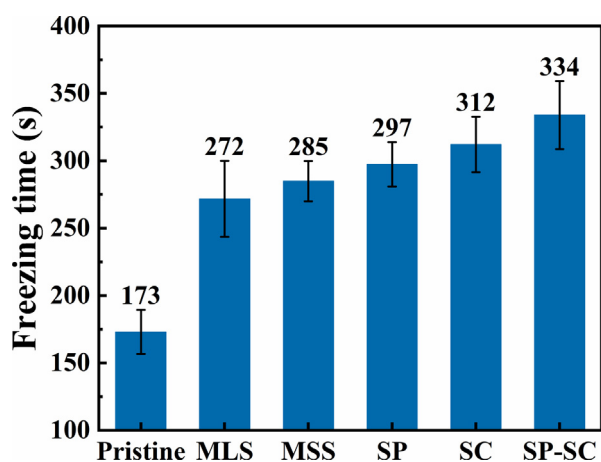


Fig. 12. Freezing times of PTFE surfaces with different structures under $-10\text{ }^{\circ}\text{C}$.

ing that the freezing time is proportional to the statistic contact angles at low temperatures. The larger the static contact angle is, the longer the corresponding freezing time is. Results show that improving the hydrophobicity of the material surface at low temperatures can effectively delay the freezing time of the water droplet. In the process of freezing, heat is mainly transferred from the water droplets to the substrates through the interface. Due to the small contact area and the air stored in the microstructures, the heat transfer rate between the droplet and the PTFE surface is effectively reduced, so the freezing time of the droplet is delayed. SC and SP-SC microstructures own the minimal contact area compared to other microstructural surfaces, which improves the anti-icing property. The smaller contact area also reduces the nucleation rate at the interface between the water droplet and the PTFE surface, thus effectively delaying the freezing of water droplets [17].

According to the classical nucleation theory [17], the total nucleation rate of the water droplet on the substrate can be expressed

$$J_{total} = J_{bulk}V + J_{w-a}S_{w-a} + J_{w-s}S_{w-s} \quad (3)$$

where, J_{bulk} , J_{w-a} , J_{w-s} represent the spontaneous nucleation rate inside water, the nucleation rate of water droplet contacting with air, and the nucleation rate of water droplets contacting with the substrate surface respectively; V , S_{w-a} , S_{w-s} represent the water droplet volume, the water droplet area contacting with air, and the water droplet and base part area, respectively. The contact part's

nucleation between the water droplet and substrate belongs to heterogeneous nucleation, while the nucleation rate inside the water droplet and the nucleation rate at the interface with the air mainly depend on the homogeneous nucleation [40]. The energy barrier of heterogeneous nucleation is much lower than homogeneous nucleation, so the overall nucleation rate mainly depends on the nucleation rate of the contact part between the water droplet and substrate, that is, mainly determined by J_{w-s} and S_{w-s} . J_{w-s} is related to the energy barrier of heterogeneous nucleation. Reducing S_{w-s} between water droplets and the surface can effectively reduce the total ice nucleation rate and delay the freezing time. Since f_s is the percentage of the actual contact area between the water droplet and the solid surface, the f_s is proportional with S_{w-s} . Table 2 shows that the values f_s of SC and SP-SC microstructures are lower than those of other morphologies, so they can effectively reduce the contact area S_{w-s} between water droplets and the substrates and the rate of ice nucleation compared to other microstructural surfaces.

4. Conclusion

By employing femtosecond laser ablation with varied fabrication parameters, the PTFE surfaces with different structures (MLS, MSS, SP, SC, SP-SC) were obtained. The two new SP and SP-SC structures fabricated on the PTFE surfaces exhibited an improved hydrophobicity in a low-temperature environment compared to conventional structures like MLS, MSS, and SP. Moreover, the freezing times on SC and SP-SC microstructure surfaces are longer than those of other microstructures. SC and SP-SC microstructures can further reduce the water-substrate contact area and enhance both the hydrophobicity and anti-icing ability of the surfaces in a low-temperature environment. The results showed that SC and SP-SC microstructures could be produced on PTFE surfaces by femtosecond laser fabrication. Later, the formation mechanism of SC and SP-SC microstructures are proposed. Building new models for various structural surfaces with condensation and frost provided a new method for analyzing the wettability in a low-temperature environment. Designing and fabricating new structures on the surfaces may be a promising way to improve the anti-icing property of superhydrophobic surfaces.

CRediT authorship contribution statement

Chengfang Ge: Writing - original draft, Investigation, Formal analysis, Data curation. **Gan Yuan:** Methodology, Supervision. **Chunlei Guo:** Conceptualization. **Chi-Vinh Ngo:** Conceptualiza-

tion, Validation, Supervision, Writing - review & editing. **Wei Li:** Writing - review & editing.

Declaration of Competing Interest

The authors declare that they have no known competing financial interests or personal relationships that could have appeared to influence the work reported in this paper.

Acknowledgments

This work was supported by National Natural Science Foundation of China (Grant No.91750205), Bill & Melinda Gates Foundation (OPP1157723), Chinese Academy of Sciences President's International Fellowship Initiative (Grant No. 2019PE0010), Strategic Priority Research Program of Chinese Academy of Sciences (XDA22010302), Jilin Provincial Science & Technology Development Project (Grant No. 20180414019GH), and K.C.Wong Education Foundation(Grant No. GJTD-2018-08).

Appendix A. Supplementary data

Supplementary data to this article can be found online at <https://doi.org/10.1016/j.matdes.2021.109689>.

References

- T.V.J. Charpentier, A. Neville, P. Millner, R.W. Hewson, A. Morina, Development of anti-icing materials by chemical tailoring of hydrophobic textured metallic surfaces, *J. Colloid Interface Sci.* 394 (2013) 539–544, <https://doi.org/10.1016/j.jcis.2012.11.021>.
- E.J. Ling, V. Uong, J.S. Renault-Crispo, A.M. Kietzig, P. Servio, Reducing ice adhesion on nonsmooth metallic surfaces: wettability and topography effects, *ACS Appl. Mater. Interfaces* 8 (13) (2016) 8789–8800, <https://doi.org/10.1021/acsami.6b00187>.
- L. Pan, F. Wang, X. Pang, L. Zhang, J. Hao, Superhydrophobicity and anti-icing of CF/PEEK composite surface with hierarchy structure, *J. Mater. Sci.* 54 (24) (2019) 14728–14741, <https://doi.org/10.1007/s10853-019-03956-0>.
- H. Zheng, S. Chang, G. Ma, S. Wang, Anti-icing performance of superhydrophobic surface fabricated by femtosecond laser composited dual-layers coating, *Energy Build.* 223 (2020), <https://doi.org/10.1016/j.enbuild.2020.110175>.
- Y. Qi, Z. Yang, W. Huang, J. Zhang, Robust superhydrophobic surface for anti-icing and cooling performance: application of fluorine-modified TiO₂ and fumed SiO₂, *Appl. Surf. Sci.* 538 (2021), <https://doi.org/10.1016/j.apsusc.2020.148131>.
- X. Tan, Y. Zhang, X. Liu, S. Xi, Z. Yan, Z. Liu, T. Shi, G. Liao, Employing micro pyramidal holes and porous nanostructures for enhancing the durability of lubricant-infused surfaces in anti-icing, *Surf. Coat. Technol.* 405 (2021), <https://doi.org/10.1016/j.surfcoat.2020.126568>.
- B. Su, Y. Tian, L. Jiang, Bioinspired interfaces with superwettability: from materials to chemistry, *J. Am. Chem. Soc.* 138 (6) (2016) 1727–1748, <https://doi.org/10.1021/jacs.5b12728>.
- L. Wang, Q.H. Gong, S.H. Zhan, L. Jiang, Y.M. Zheng, Robust Anti-Icing Performance of a Flexible Superhydrophobic Surface, *Adv. Mater.* 28(35) (2016) 7729–+. Doi: [10.1002/adma.201602480](https://doi.org/10.1002/adma.201602480).
- Z. Zhan, Z. Li, X. Li, E. Garcell, S. Singh, M. ElKabbash, C. Guo, Creating superhydrophobic polymer surfaces with superstrong resistance to harsh cleaning and mechanical abrasion fabricated by scalable one-step thermal-imprinting, *Adv. Mater. Interfaces* 6 (16) (2019) 1900240, <https://doi.org/10.1002/admi.201900240>.
- D. Wang, Q. Sun, M.J. Hokkanen, C. Zhang, F.Y. Lin, Q. Liu, S.P. Zhu, T. Zhou, Q. Chang, B. He, Q. Zhou, L. Chen, Z. Wang, R.H.A. Ras, X. Deng, Design of robust superhydrophobic surfaces, *Nature* 582 (7810) (2020) 55–59, <https://doi.org/10.1038/s41586-020-2331-8>.
- W. Barthlott, C. Neinhuis, Purity of the sacred lotus, or escape from contamination in biological surfaces, *Planta* 202 (1) (1997) 1–8, <https://doi.org/10.1007/s004250050096>.
- A.O. Ijaola, E.A. Bamidele, C.J. Akisin, I.T. Bello, A.T. Oyatobo, A. Abdulkareem, P. K. Farayibi, E. Asmatulu, Wettability transition for laser textured surfaces: a comprehensive review, *Surfaces and Interfaces* 21 (2020), <https://doi.org/10.1016/j.surfin.2020.100802>.
- W. Xing, Z. Li, H. Yang, X. Li, X. Wang, N. Li, Anti-icing aluminum alloy surface with multi-level micro-nano textures constructed by picosecond laser, *Mater. Des.* 183 (2019) 108156, <https://doi.org/10.1016/j.matdes.2019.108156>.
- L. Cao, A.K. Jones, V.K. Sikka, J. Wu, D. Gao, Anti-icing superhydrophobic coatings, *Langmuir* 25 (21) (2009) 12444–12448, <https://doi.org/10.1021/la902882b>.
- M. Ruan, W. Li, B. Wang, B. Deng, F. Ma, Z. Yu, Preparation and anti-icing behavior of superhydrophobic surfaces on aluminum alloy substrates, *Langmuir* 29 (27) (2013) 8482–8491, <https://doi.org/10.1021/la400979d>.
- P. Guo, Y. Zheng, M. Wen, C. Song, Y. Lin, L. Jiang, Icephobic/anti-icing properties of micro/nanostructured surfaces, *Adv. Mater.* 24 (19) (2012) 2642–2648, <https://doi.org/10.1002/adma.201104412>.
- A. Alizadeh, M. Yamada, R. Li, W. Shang, S. Otta, S. Zhong, L. Ge, A. Dhinojwala, K.R. Conway, V. Bahadur, A.J. Vinciguerra, B. Stephens, M.L. Blohm, Dynamics of ice nucleation on water repellent surfaces, *Langmuir* 28 (6) (2012) 3180–3186, <https://doi.org/10.1021/la2045256>.
- Y. Zhang, E. Anim-Danso, S. Bekele, A. Dhinojwala, Effect of surface energy on freezing temperature of water, *ACS Appl. Mater. Interfaces* 8 (27) (2016) 17583–17590, <https://doi.org/10.1021/acsami.6b02094>.
- S.A. Kulinich, S. Farhadi, K. Nose, X.W. Du, Superhydrophobic surfaces: are they really ice-repellent?, *Langmuir* 27 (1) (2011) 25–29, <https://doi.org/10.1021/la104277q>.
- S. Jung, M. Dorrestijn, D. Raps, A. Das, C.M. Megaridis, D. Poulikakos, Are superhydrophobic surfaces best for icephobicity?, *Langmuir* 27 (6) (2011) 3059–3066, <https://doi.org/10.1021/la104762g>.
- J.Y. Lv, Y.L. Song, L. Jiang, J.J. Wang, Bio-inspired strategies for anti-icing, *ACS Nano* 8 (4) (2014) 3152–3169, <https://doi.org/10.1021/nn406522n>.
- L. Jiang, A.D. Wang, B. Li, T.H. Cui, Y.F. Lu, Electrons dynamics control by shaping femtosecond laser pulses in micro/nanofabrication: modeling, method, measurement and application, *Light Sci. Appl.* 7 (2018) 17134, <https://doi.org/10.1038/lsa.2017.134>.
- Z. Qin, J. Ai, Q. Du, J. Liu, X. Zeng, Superhydrophobic polytetrafluoroethylene surfaces with accurately and continuously tunable water adhesion fabricated by picosecond laser direct ablation, *Mater. Des.* 173 (2019), <https://doi.org/10.1016/j.matdes.2019.107782>.
- Y.L. Zhan, M. Ruan, W. Li, H. Li, L.Y. Hu, F.M. Ma, Z.L. Yu, W. Feng, Fabrication of anisotropic PTFE superhydrophobic surfaces using laser microprocessing and their self-cleaning and anti-icing behavior, *Colloids Surf. Physicochem. Eng. Aspects* 535 (2017) 8–15, <https://doi.org/10.1016/j.colsurfa.2017.09.018>.
- H.J. Kwon, J. Yeo, J.E. Jang, C.P. Grigoropoulos, J.H. Yoo, Single pass laser process for super-hydrophobic flexible surfaces with micro/nano hierarchical structures, *Materials (Basel)* 11 (7) (2018), <https://doi.org/10.3390/ma11071226>.
- J.H. Yoo, H.J. Kwon, D. Paeng, J. Yeo, S. Elhadji, C.P. Grigoropoulos, Facile fabrication of a superhydrophobic cage by laser direct writing for site-specific colloidal self-assembled photonic crystal, *Nanotechnology* 27 (14) (2016) 145604, <https://doi.org/10.1088/0957-4484/27/14/145604>.
- K. Yin, H. Du, Z. Luo, X. Dong, J.-A. Duan, Multifunctional micro/nano-patterned PTFE near-superamphiphobic surfaces achieved by a femtosecond laser, *Surf. Coat. Technol.* 345 (2018) 53–60, <https://doi.org/10.1016/j.surfcoat.2018.04.010>.
- D. Chu, S.C. Singh, J. Yong, Z. Zhan, X. Sun, J.A. Duan, C. Guo, Superamphiphobic surfaces with controllable adhesion fabricated by femtosecond laser beam on PTFE, *Adv. Mater. Interfaces* 6 (14) (2019) 1900550, <https://doi.org/10.1002/admi.201900550>.
- C.-E. Athanasiou, M.-O. Hongler, Y. Bellouard, Unraveling brittle-fracture statistics from intermittent patterns formed during femtosecond laser exposure, *Phys. Rev. Appl.* 8 (5) (2017), <https://doi.org/10.1103/PhysRevApplied.8.054013>.
- D.B. Wolfe, J.B. Ashcom, J.C. Hwang, C.B. Schaffer, E. Mazur, G.M. Whitesides, Customization of poly(dimethylsiloxane) stamps by micromachining using a femtosecond-pulsed laser, *Adv. Mater.* 15(1) (2003) 62–+. Doi: [10.1002/adma.200390012](https://doi.org/10.1002/adma.200390012).
- J. Yong, J. Huo, Q. Yang, F. Chen, Y. Fang, X. Wu, L. Liu, X. Lu, J. Zhang, X. Hou, Femtosecond laser direct writing of porous network microstructures for fabricating super-slippy surfaces with excellent liquid repellence and anti-cell proliferation, *Adv. Mater. Interfaces* 5 (7) (2018), <https://doi.org/10.1002/admi.201701479>.
- R.L. Harzic, H. Schuck, D. Sauer, T. Anhut, I. Riemann, K. König, Sub-100 nm nanostructuring of silicon by ultrashort laser pulses, *Opt. Express* 13 (17) (2005) 6651–6656, <https://doi.org/10.1364/OPEX.13.006651>.
- J. Krüger, S. Martin, H. Mädebach, L. Urech, T. Lippert, A. Wokaun, W. Kautek, Femto- and nanosecond laser treatment of doped polymethylmethacrylate, *Appl. Surf. Sci.* 247 (1–4) (2005) 406–411, <https://doi.org/10.1016/j.apsusc.2005.01.078>.
- A.Y. Vorobyev, C. Guo, Direct femtosecond laser surface nano/microstructuring and its applications, *Laser Photonics Rev.* 7 (3) (2013) 385–407, <https://doi.org/10.1002/lpor.201200017>.
- J. Ji Nivas, S. He, Z. Song, A. Rubano, A. Vecchione, D. Paparo, L. Marrucci, R. Bruzzese, S. Amoroso, Femtosecond laser surface structuring of silicon with Gaussian and optical vortex beams, *Appl. Surf. Sci.* 418 (2017) 565–571, <https://doi.org/10.1016/j.apsusc.2016.10.162>.
- Y. Fang, J. Yong, F. Chen, J. Huo, Q. Yang, H. Bian, G. Du, X. Hou, Durability of the tunable adhesive superhydrophobic PTFE surfaces for harsh environment applications, *Appl. Phys. A* 122 (9) (2016), <https://doi.org/10.1007/s00339-016-0325-z>.
- K.K. Varanasi, T. Deng, J.D. Smith, M. Hsu, N. Bhate, Frost formation and ice adhesion on superhydrophobic surfaces, *Appl. Phys. Lett.* 97 (23) (2010) 234102, <https://doi.org/10.1063/1.3524513>.

- [38] J.P. Hindmarsh, A.B. Russell, X.D. Chen, Experimental and numerical analysis of the temperature transition of a suspended freezing water droplet, *Int. J. Heat Mass Transfer* 46 (7) (2003) 1199–1213, [https://doi.org/10.1016/S0017-9310\(02\)00399-X](https://doi.org/10.1016/S0017-9310(02)00399-X).
- [39] H. Peng, Q. Wang, T. Wang, L. Li, Z. Xia, J. Du, B. Zheng, H. Zhou, L. Ye, Study on dynamics and freezing behaviors of water droplet on superhydrophobic aluminum surface, *Appl. Phys. A* 126 (10) (2020), <https://doi.org/10.1007/s00339-020-04003-5>.
- [40] Q. Li, Z. Guo, Fundamentals of icing and common strategies for designing biomimetic anti-icing surfaces, *J. Mater. Chem. A* 6 (28) (2018) 13549–13581, <https://doi.org/10.1039/c8ta03259a>.